

## Article

# Land Cover Classification in the Antioquia Region of the Tropical Andes Using NICFI Satellite Data Program Imagery and Semantic Segmentation Techniques

Luisa F. Gomez-Ossa <sup>1,\*</sup>, German Sanchez-Torres <sup>2</sup> and John W. Branch-Bedoya <sup>1</sup><sup>1</sup> Facultad de Minas, Universidad Nacional de Colombia, Medellín 050041, Colombia; jwbranch@unal.edu.co<sup>2</sup> Facultad de Ingenierías, Universidad del Magdalena, Santa Marta 470004, Colombia; gsanchez@unimagdalena.edu.co

\* Correspondence: lfgomezos@unal.edu.co

**Abstract:** Land cover classification, generated from satellite imagery through semantic segmentation, has become fundamental for monitoring land use and land cover change (LULCC). The tropical Andes territory provides opportunities due to its significance in the provision of ecosystem services. However, the lack of reliable data for this region, coupled with challenges arising from its mountainous topography and diverse ecosystems, hinders the description of its coverage. Therefore, this research proposes the Tropical Andes Land Cover Dataset (TALANDCOVER). It is constructed from three sample strategies: aleatory, minimum 50%, and 70% of representation per class, which address imbalanced geographic data. Additionally, the U-Net deep learning model is applied for enhanced and tailored classification of land covers. Using high-resolution data from the NICFI program, our analysis focuses on the Department of Antioquia in Colombia. The TALANDCOVER dataset, presented in TIF format, comprises multiband R-G-B-NIR images paired with six labels (dense forest, grasslands, heterogeneous agricultural areas, bodies of water, built-up areas, and bare-degraded lands) with an estimated 0.76 F1 score compared to ground truth data by expert knowledge and surpassing the precision of existing global cover maps for the study area. To the best of our knowledge, this work is a pioneer in its release of open-source data for segmenting coverages with pixel-wise labeled NICFI imagery at a 4.77 m resolution. The experiments carried out with the application of the sample strategies and models show F1 score values of 0.70, 0.72, and 0.74 for aleatory, balanced 50%, and balanced 70%, respectively, over the expert segmented sample (ground truth), which suggests that the personalized application of our deep learning model, together with the TALANDCOVER dataset offers different possibilities that facilitate the training of deep architectures for the classification of large-scale covers in complex areas, such as the tropical Andes. This advance has significant potential for decision making, emphasizing sustainable land use and the conservation of natural resources.

**Keywords:** semantic segmentation; land cover classification; tropical Andean region; U-Net convolutional network; Colombia



**Citation:** Gomez-Ossa, L.F.; Sanchez-Torres, G.; Branch-Bedoya, J.W. Land Cover Classification in the Antioquia Region of the Tropical Andes Using NICFI Satellite Data Program Imagery and Semantic Segmentation Techniques. *Data* **2023**, *8*, 185. <https://doi.org/10.3390/data8120185>

Academic Editor: Juan-Carlos Jiménez-Muñoz

Received: 3 October 2023

Revised: 2 November 2023

Accepted: 6 November 2023

Published: 4 December 2023



**Copyright:** © 2023 by the authors. Licensee MDPI, Basel, Switzerland. This article is an open access article distributed under the terms and conditions of the Creative Commons Attribution (CC BY) license (<https://creativecommons.org/licenses/by/4.0/>).

## 1. Introduction

Satellite images are a highly valuable information source for land cover segmentation, an essential task for sustainable development, agriculture, forestry, and urban planning. Compared to images typically used in computer vision, this information source is under-researched in the deep learning (DL) area [1]. However, in recent years, significant advances have been made [2], and their availability on a global, regional, and local scale enable not only the construction of large training sets but also the evaluation of the performance of different DL architectures.

Specifically, studies have been conducted with medium and low-resolution images (30–500 m) [3–5]. Based on the improved spatial and temporal resolution of data from [6]

and the analytical capabilities available for image processing, there is potential to establish new datasets and machine learning models (ML) [7,8]. Some examples of empirical methods are currently being used to monitor compliance with the Sustainable Development Goals (SDGs) for the year 2030 [9,10].

Datasets for training machine-learning-based models have predominantly been constructed in European geographic contexts or high-latitude zones [11], and for specific tasks of image classification and object detection. Concurrently, the primary study objective corresponds to urban areas [12,13]. Therefore, it is crucial to direct research efforts towards rural areas using data representing the geographic diversity of the tropical region, specifically mountainous areas like the Andean region, given its importance in the provision of ecosystem services on which the population depends [14–16].

Several datasets have been proposed in the literature, such as SENT12MS [17], BigEarthNet [18], and MLRSNet [19]. Advances in computer vision, particularly in the areas of object detection and scene classification [12], have been made possible thanks to the availability of these datasets. In addition to these areas, in semantic segmentation, it is important to have a pixel-level labeled dataset [12], a complex task in which images originating from remote sensors are highly dependent on expert knowledge. The accuracy of the algorithms is highly dependent on the number of classes considered, as well as the spectral/spatial distinction between classes [12,20].

In order to improve the application of DL models, primarily in the tropical region, the TALANDCOVER dataset (Tropical Andes Land Cover Dataset) is proposed using different strategies to deal with imbalanced geographic data. The dataset pertains to the department of Antioquia, Colombia and was developed with the NICFI satellite data program. This program provides complimentary access to high-spatial-resolution mosaics (4.7 m) optimized for analysis in the tropical region, offering substantial potential for mapping cover in extensively transformed ecosystems. The dataset comprises multiband R-G-B-NIR images for training and testing, in addition to the label masks associated with six covers: dense forest, grasslands, heterogeneous agricultural areas, bodies of water, built-up areas, and bare-degraded lands.

## 2. Previous Work

In the field of remote sensing, the classification of observed data has conventionally been executed through manual means, based on expert knowledge. However, this approach presents a constraint due to the vast amount of information that needs to be processed [21,22]. A potential approach could involve the training of a computational artificial intelligence (AI)-based model through the utilization of expert-provided labels, which would enable the autonomous prediction of diverse land cover categories.

The ISPRS project (International Society for Photogrammetry and Remote Sensing) [13,23] with the Vaihingen and Potsdam datasets has been instrumental in advancing the field of semantic segmentation by being pioneers in providing an open-access dataset with labeled satellite images. Other datasets, such as SpaceNet [24], DynamicEarthNet [25], Dynamic World [26], and ESA WorldCover [27], have made noteworthy contributions to the field of semantic segmentation and the global mapping of land cover; however, due to their global scale, local patterns could be missed. Studies with specific data, from a particular geographical area, which in Latin America has been carried out mainly in Brazil [28,29], could contribute and be a complement to the construction of new models or used for the validation of existing ones.

The utilization of statistical classifiers, such as maximum likelihood [30], was one of the initial methods adopted for satellite image categorization following the establishment of the Landsat program in 1972. The maximum likelihood method employs a supervised classification technique, assuming that the spectral characteristics of each class adhere to a Gaussian distribution [31]. Recent research has employed this classifier and is prevalent in the remote sensing field; however, it necessitates assumptions about data distribution and

demonstrates overfitting for the more representative classes [4,5,32,33]. Such constraints underline the requirement for more advanced methods, such as ML or DL [5,34].

There exists a substantial body of research in which various ML methods have been compared for land cover classification and change prediction based on satellite imagery [35–39]. The studies conducted emphasize superior accuracy with the random forests method [40]. This method has been further explored with different sample configurations and hyperparameter combinations [41] and employed to ascertain the significance of a set of predictor variables based on the respective evaluation criterion [42,43]. Random forests can depict nonlinear relationships, are relatively insensitive to correlated predictors and have been successfully applied in various remote sensing contexts [44].

Satellite imagery has been effectively analyzed using other conventional classification algorithms, such as support vector machines (SVMs) and multilayer perceptrons (MLPs). Since 2014, advances in DL have received greater attention from the remote sensing community due to the ability that different architectures have shown in pattern recognition, such as convolutional neural networks (CNNs) [45], recurrent neural networks (RNNs) [46], and autoencoders (AEs) [47], among others, which marked a significant turning point in the field of DL [12].

The efficacy of CNNs in domains that are inherent to computer vision has resulted in the assimilation and amplification of these networks for addressing issues in the realm of remote sensing, as per the findings in [2]. According to the reference framework, CNNs have gained significant popularity owing to their ability to process data in the form of multiple matrices [48]. This makes them a suitable choice for processing multiband images that have regular arrays of pixels. Moreover, deep learning algorithms exhibit the capability to capture nonlinear patterns in spatial and temporal domains [49].

The U-Net framework, which is frequently utilized in the segmentation of medical images [50], has been applied in multiple research endeavors involving satellite imagery, demonstrating satisfactory outcomes. According to [51], a level of accuracy of around 90% was attained in the mapping of the occurrence or non-occurrence of trees and shrubs in Queensland, Australia. In [52], a comparative study of three distinct architectures, namely U-Net, ResNet, and DenseNet, was conducted to map forested and non-forested regions utilizing radar imagery. The findings indicate that the U-Net framework exhibited enhanced accuracy. Several studies and comparative analyses [28] have documented better performance of U-Net in comparison to conventional techniques [49,53,54] and other CNN architectures. Diverse studies emphasize the significance of algorithm design in the effective classification of multiple classes or types of land cover.

Furthermore, the efficacy of U-Net for the task of satellite image segmentation has promoted its investigation. In [55] introduced an integrated framework that combines enhanced versions of the U-Net and SegNet models to enhance the accuracy and performance of high-resolution image segmentation. Enhanced versions of U-Net have been utilized to analyze the spatial distribution of palm canopy and its relationship with human disturbance and soil conditions [56]; they have also been employed for the assessment of mining activities, a primary cause of deforestation, land use change, and pollution [57], as well as for mapping the inundation status of forested wetlands by integrating spectral bands, topographic data, and lidar information [58].

CNN architectures require a large amount of data for training [59], and the construction of a labeled dataset for coverage segmentation from satellite image represents a challenge [20]. Despite the great efforts that have been made and the existence of different datasets [11,19], a strong bias in the literature has been developed toward urban areas [12] in the Northern Hemisphere. Thus, the tropical Andes region is underrepresented, which hinders the development of models that help monitoring LULCC. On the other hand, careful choice and preprocessing of data are crucial to avoid unwanted biases in the models. TALANDCOVER, in addition to representing a tropical mountainous region, presents sampling strategies as a different option to the data augmentation method used in DL [60,61] for addressing imbalanced data, allowing exploration and comparative analysis, not only

between datasets but also between architectures and fine-tuning processes with the aim of obtaining models with greater generalization capacity, which adapt to the geographical characteristics of the study area.

The plethora of sensors available and their variations in spectral and spatial characteristics present an opportunity for mapping, quantifying, and detecting changes through DL methods. Recent studies encompass the analysis of various sensors [62,63] and spectral bands, finding the NIR and SWIR bands to be of greater significance in land cover classification. Conversely, the blue band was identified as the least significant variable. In [49,64], DL was employed for optical and fused classification using synthetic aperture radar (SAR) imagery; these studies demonstrated that when using combined data, the accuracy surpasses that of individual datasets. In [65], the potential in the joint analysis of multiple sensors for delineating forest cover across various ecosystems located in Germany was highlighted.

Recently, the dataset from the NICFI program was published, in which various organizations, including Planet, Airbus, and Kongsberg Satellite Service, released free and analysis-ready high-resolution base maps (4.77 m per pixel). This dataset serve as a valuable information source for monitoring landscapes in tropical areas; however, only a few studies have utilized these data, and notable examples in Latin America include those in Brazil, aiming to predict the mortality risk of trees in eucalyptus forests [66] and for land cover classification using random forests [63], as well as in Peru, which assessed the dataset's efficacy in land cover mapping. At the continental level, efforts are underway in Africa [67,68].

The study of image segmentation is a subject that has been extensively researched. The Segment Anything Model (SAM) was recently introduced [69], this model has demonstrated impressive performance in various tasks and has outperformed fully supervised approaches. Especially in the fields of geography, remote sensing, and segmentation of high-spatial-resolution images (orthophotos), the SAM proves to be effective [70]. Despite the limited application of this model in satellite imagery, additional experimentation is required, particularly in the optimization of hyperparameters. Nevertheless, the SAM presents a promising avenue for the automatic generation of masks as input for the creation of labeled data and the development of DL models like U-Net.

### 3. Materials and Methods

The general methodology employed in this study consists of five stages, encompassing the collection of raw satellite images, which are preprocessed and labeled in the following two phases. Subsequently, a DL model was designed and trained in the subsequent stage, and the performance was evaluated using a set of carefully selected metrics, considering the task of semantic segmentation and accounting for the high levels of class imbalance present in the data (see Figure 1).

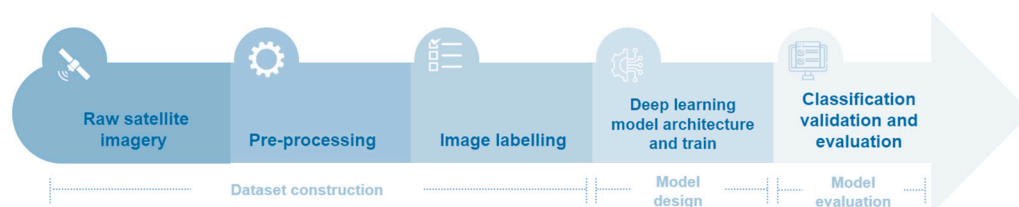


**Figure 1.** General methodology.

#### 3.1. Study Area Definition

The Department of Antioquia in Colombia is in the northwest region of the country. Its geographic coordinates span from approximately 5.4° N to 8.8° N latitude and 73.8° W to 77.5° W longitude (see Figure 2). It spans an area of approximately 63,612 km<sup>2</sup>. It is bordered by several neighboring departments, including Cordoba and Bolivar to the north, Santander and Boyacá to the east, Caldas y Risaralda to the south, and Chocó to the west.

The Antioquia department has a significant administrative division within the country, comprising 125 municipalities and serving as a relevant economic and cultural hub in Colombia.

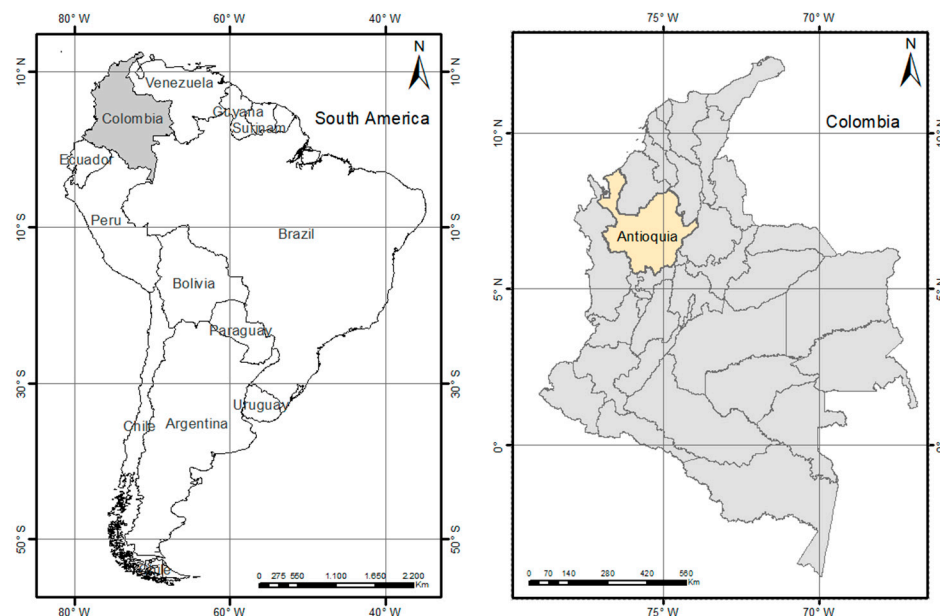


**Figure 2.** Geographical Location of the Study Region.

Land use patterns in Antioquia reflect its economic importance and environmental diversity. The department ranges from mountainous regions, dense forests, and protected areas to fertile valleys and extensive agricultural lands that include coffee plantations, banana zones, and cattle grazing areas.

During the period of 1990 to 2015, the forest cover in Antioquia decreased from 2,700,000 ha to 2,212,000 ha [71], with an approximate annual loss of 19,520 ha. For the Andean forest (>1000 m above sea level), it is reported that the coverage decreased from 1,210,000 ha to 530,000 ha over the same twenty-five (25) year period; this signifies a reduction of 56.19%, with an annual deforestation rate of 27,200 ha, making it one of the most affected ecosystems, following dry forests [71].

In the department, new road infrastructure projects have been developed, aiming to enhance connectivity with the north of the country [72]. Additionally, it is the leading gold producer in Colombia [73]. This range of conditions and socioeconomic dynamics make it a significant area for the analysis of LULCC based on high-spatial-resolution imagery.

### 3.2. Raw Satellite Imagery

Numerous Earth observation programs provide open-access datasets, such as NASA's Landsat and ESA's (European Space Agency) Copernicus, and the products of this programs were among the first to be explored due to their availability and have been the primary input in constructing datasets for training deep networks in classification and object detection tasks [74]. In Brazil, progress has been made, consolidating a dataset with images classified in a binary manner (forest, non-forest) [28], which limits data use. Therefore, with this research, we aim to have an open-access, labeled dataset that represents the geographical diversity of classes in the tropical region.

Recently, in 2020, images from the NICFI satellite data program were published. This initiative aims to provide support for reducing tropical forest loss. It represents the first open-access dataset at a resolution of 4.77 m, covering the entire tropical region between 30° north and 30° south, encompassing approximately 45 million square kilometers [75]; therefore, given its characteristics, such as a higher spatial resolution, with respect to other

products, spectral resolution (red–green–blue near infrared), availability, and geographic coverage, NICFI images were chosen for the development of the present investigation.

### 3.3. Preprocessing

A Python script was written in conjunction with the Planet Scope API to access tiles based on the data and boundary box of the Antioquia department in Colombia. This resulted in an acquisition of approximately 392 tiles. These tiles correspond to composite images taken in the first half of 2019, with the specific product being ‘planet\_medres\_normalized\_analytic\_2018-12\_2019-05\_mosaic’. This product was chosen since its dates align well with available land cover maps, which were used to construct the image labels. After filtering the tiles using the study area’s geometry, a final set of 114 tiles was identified. These tiles are entirely encapsulated within the predetermined study area, with each tile measuring  $4096 \times 4096$  pixels.

To ensure compatibility with deep learning models, each tile was divided into image sections with dimensions of  $128 \times 128$  pixels. Typically, datasets used for training deep learning models have dimensions that align with powers of two (e.g., 128, 256, 512). Dimensions of  $128 \times 128$  were chosen to strike a balance between the volume of training data and the spatial context size [76]. Additionally, a random selection of approximately 5% of the image sections contained within the 114 tiles was conducted. This was conducted with the intent of constructing a random dataset for model training (see Figure 3).

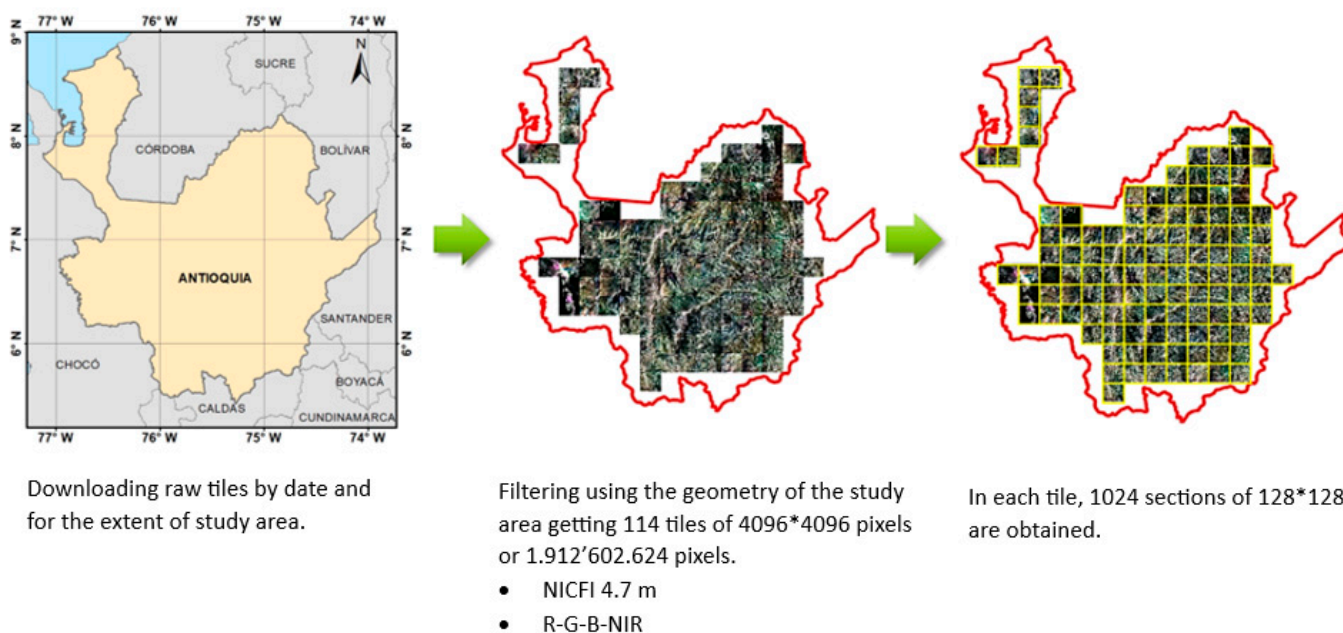


**Figure 3.** Methodological Framework for the Preprocessing and Generation of a Random Dataset.

#### 3.3.1. Image Labelling

The construction of a labeled dataset for training is very important for land cover mapping at fine spatial resolution. Field data collection has the highest accuracy and reliability; however, this method is costly and time-consuming, especially for both long-term and large-scale land cover mapping. Additionally, fieldwork limitations exist in some areas with public order problems. In fact, visual interpretation or the use of open data, such as existing coverage maps, are currently the most widely used data collection method [68,77].

Recently, the ESRI (Environmental Systems Research Institute) [78], the European Agency-ESA [27], Google [26], and the University of Maryland-Global Land Analysis and Discovery (GLAD) laboratory [79] have published global cover maps using Sentinel and Landsat images. These layers constitute a valuable input for the analysis of LULCC, and

compared to other global products (Copernicus Global Land Cover 100, MODIS Land Cover Type Yearly Global 500 m), they present better spatial resolution (<100 m).

On the other hand, there are forest cover products (forest/non-forest) at a global level with spatial resolutions of 50 m [80], 30 m [81], and 25 m [82], which represent a very valuable contribution to the monitoring of forests in the tropical region. However, some studies when comparing global maps with local maps show an overestimation of forest cover [83].

In [28], a dataset for monitoring the Amazon rainforest based on Sentinel images (10 m) with the R-G-B-NIR bands and a binary forest/non-forest label was constructed; however, the study acknowledges certain limitations, such as the relatively small size of the dataset, which can impact the performance of certain CNN architectures. Additionally, the authors consider that the binary label is not an optimal solution in terms of the applicability of the results.

This paper, in contrast to the previously described approaches, presents a higher spatial resolution (4.7 m) and a pixel-wise multiclass label representing six types of land cover. In general, promoting analysis with high-resolution satellite images and continuous monitoring is essential throughout the tropical region to evaluate trends in LULCC.

To associate a pixel-level label with the  $128 \times 128$  image sections, we reviewed the characteristics of different datasets and the availability of land cover layers. Figure 4 presents a scheme that summarizes the main characteristics of the products selected in the previous evaluation.

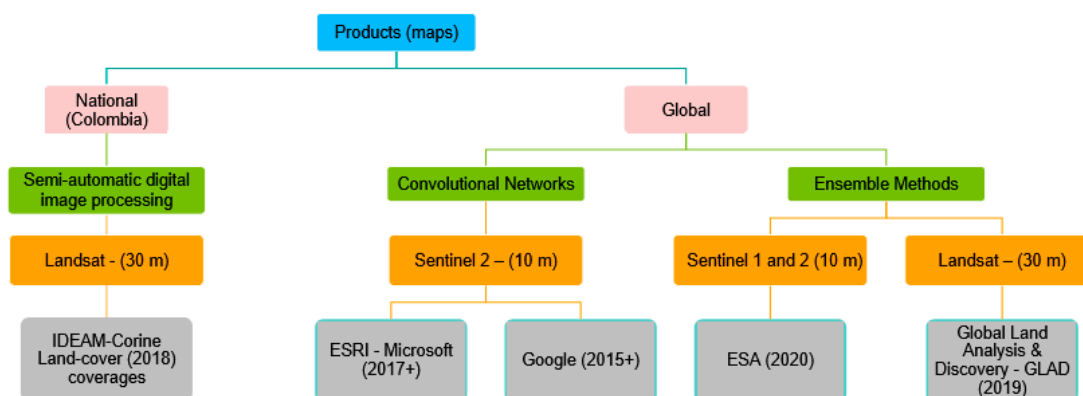


**Figure 4.** Analysis of Remote Sensing, National and Global Coverage Data Sources. Map extent (pink), methodology used in the construction of the maps (green), type of images (orange), and responsible organization (grey).

To compare the selected products and define which of them is the most suitable for the construction of the label, the products were reclassified into 6 classes according to the geographical characteristics of the study area.

- *Bare-degraded land*: corresponds to terrain surfaces devoid of vegetation or with scant vegetation cover due to the occurrence of natural and human-induced processes.
- *Dense forest*: corresponds to a vegetation community dominated by typical tree elements, which form a continuous or semi-continuous canopy.
- *Agricultural heterogeneous areas*: corresponds to areas dedicated to permanent, transient, and mixed crops with natural spaces, such as open tree cover.
- *Grasslands*: corresponds to lands where pastures have been structured with little vegetation presence.
- *Water bodies*: corresponds to permanent bodies of water.
- *Built-up areas*: corresponds to territories covered by urban areas, including parks and urban green areas.

To select the dataset to be used as the backbone of this research, a test of the level of agreement between the global covers and the expert sampled images interpretation was conducted. In total, 174 images, equivalent to 2,850,816 pixels, were digitized.

### 3.3.2. Construction of Balanced Dataset

In ML, it is common to perform random sampling to construct a training set. However, applying this type of sampling in the analysis of geographical data from satellite images is not appropriate due to the issue of class imbalance. Different strategies have been proposed in the literature to address the problem of imbalance, both from data augmentation techniques [60,61] and from models with new loss functions [84].

In this investigation, to ensure that all land cover classes have sufficient representation, a sampling strategy called minimum percentage per class was employed. This means that each class has a minimum percentage of representation in each image section; for this, the present work employs a georeferenced sliding window technique to scan images and identify specific sections that meet a predetermined minimum threshold of a chosen land cover category. Simultaneously, the sliding window eliminates sections that display any form of overlap.

The identification and categorization of land cover classes is based on their level of representativeness within the images. Using a sliding window approach, a predetermined number of image segments is identified based on land cover thresholds, set at both 50% and 70%. The dataset construction process involves selecting the minimum number of image sections by class that meet the established threshold and the number of images corresponding to the least represented class.

As a crucial component of the quality assessment procedure, image segments that contain inaccuracies, such as uniform pixel values throughout the image, are methodically eliminated.

The image sections that have been selected are then divided into two datasets, namely training and test datasets, with a ratio of 80% for training and 20% for testing. This ratio guarantees that the deep learning algorithm is provided with a sufficient amount of data to facilitate learning [85], while simultaneously preserving a distinct dataset for the purpose of validating its performance. It is important to highlight that the testing data were not used for any training purposes and were only used for accuracy assessment.

### 3.4. Deep Learning Model Architecture and Train

Several DL architectures have been developed with the specific purpose of segmenting satellite images [2]. Regardless of the type of architecture employed, it is necessary to consider crucial factors, such as class imbalance and the availability of data for training.

In the present study, a U-Net-like network was proposed based on [50]. The network is founded on convolutional architectures and encompasses four stages of contraction and expansion (see Figure 5). The development of the model was executed utilizing the programming language Python, as well as the Keras [86] and Tensorflow [87] libraries. The model was adapted to accommodate the input data dimensions of  $128 \times 128$ . We introduced modifications to the number of filters, ranging from 16 to 128, and incorporated dropout techniques with values of 0.1 and 0.2 in the convolutional layers to address the issue of overfitting.

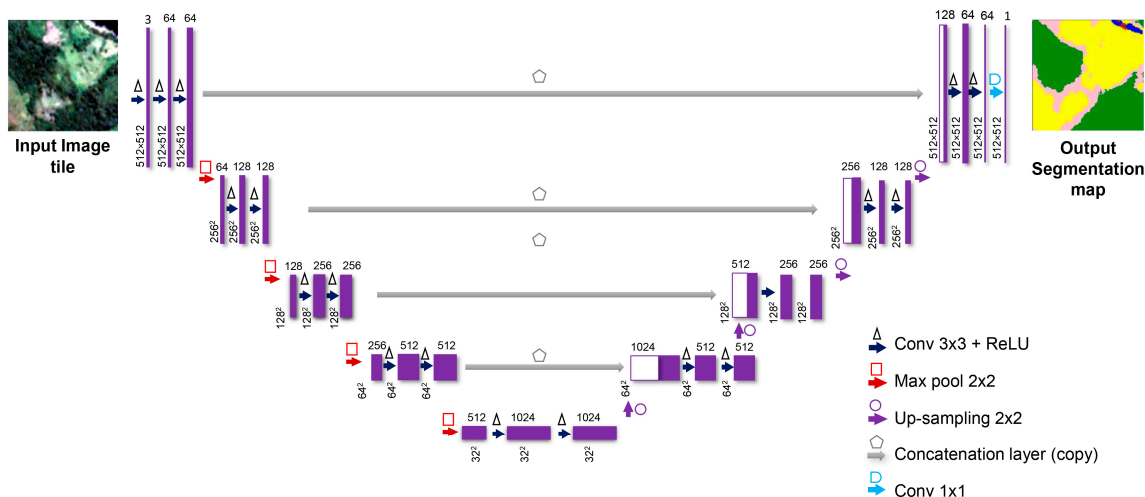


Figure 5. Architectural Schematic of the Deep Learning Model.

Preprocessing procedures were executed on the data prior to the training phase. The data were standardized through a process of subtracting the mean value of each band and dividing it by its corresponding standard deviation. This could help to address possible instabilities in training arising from the different input data scale and the difference in lighting conditions and could make the model less sensitive to outliers compared to min–max scaling [88]. Furthermore, we employed Keras he\_normal initializer without incorporating a specific seed value. Consequently, there are pragmatic discrepancies in the weight initialization process for all the models.

### 3.5. Classification Validation and Evaluation

In order to evaluate the performance of the proposed land cover classification model, several metrics are used. Considering land cover classification as a highly unbalanced problem, it is important to use metrics that can handle the class imbalance effectively.

The F1 score is used as the primary metric for evaluating the model’s performance. The F1 score is a measure of the balance between precision and recall, and it provides a single metric that combines both of these important aspects into a single value.

$$Precision = \frac{True\ Positives}{(True\ Positives + False\ Positives)} \tag{1}$$

$$Recall = \frac{True\ Positives}{(True\ Positives + False\ Negatives)} \tag{2}$$

$$F1 = \frac{2(Precision)(Recall)}{(Precision + Recall)} \tag{3}$$

$$mIoU = \frac{1}{N} \sum_{i=1}^N \frac{TP_i}{TP_i + FP_i + FN_i} \tag{4}$$

Other metrics, such as precision, recall, and Intersection over Union are also used to assess the model’s performance. Precision measures the proportion of true positive predictions out of all positive predictions, while recall measures the proportion of true positive predictions out of all actual positive cases.

## 4. Results

### 4.1. Image Labelling

Regarding the evaluation of the selected products for the construction of the label, the following analysis is obtained (see Figure 6).

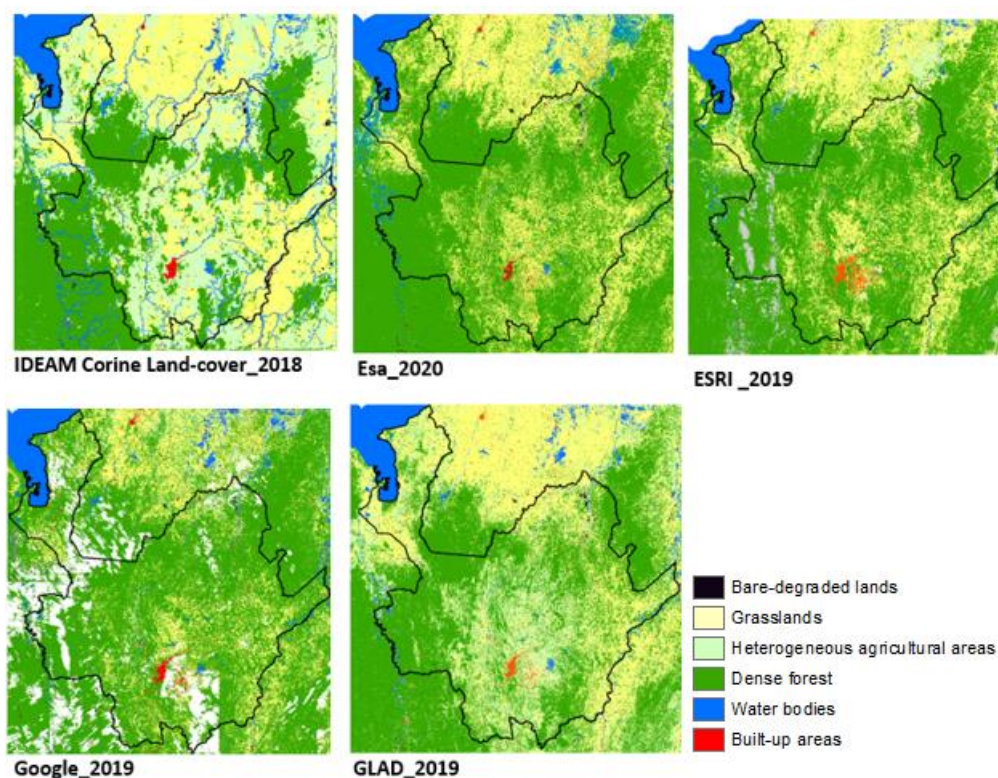


**Figure 6.** Comparison of the evaluated product.

The national map (Corine Land Cover) was discarded because its vector format is at a scale of 1:100,000 and with a minimum mappable area of 25 ha for rural areas [89]. Therefore, detail and precision are lost when converting the national map to raster, and given its coarse scale, we consider it incompatible with what is interpreted in the 4.77 m NICFI images.

According to the visual interpretation of the NICFI images in true color (RGB) and false color (NIR-R-G), the ESA map overestimates both grasslands and forest in agricultural areas. On the contrary, small areas and linear shapes that are part of the water bodies present a better delimitation (see Figure 6).

The ESRI map shows cloud coverage towards the west area; likewise, the Google map, which was built in Google Earth Engine with a composite of images for the year 2019, does not yield classification results on several sectors since according to the methodology proposed by Google [26], a filter is performed which discards pixels that exceed 35% cloud cover within a given period of time. Both the ESRI and Google maps overestimate the urban area and forest cover over agricultural areas.

In general, a greater overestimation in forest cover is observed for the ESA, ESRI, and Google maps. A possible reason for this is the technical challenge of separating the woody and herbaceous components [90], although a more rigorous evaluation is required. There are several studies that highlight the difficulties of individually applying global coverage maps at the regional level [68,83].

The label construction (Talandcover map) was based on the GLAD map (Global Land Analysis and Discovery) [76] and the ESA map [27] (see Table 1). The GLAD map was chosen because it incorporates information on canopy height [81] and vegetation cover percentage. It offers greater flexibility in delineating dense forest cover compared to other products that solely rely on spectral information and that consider only a few cover classes. The ESA map, on the other hand, utilizing radar images such as Sentinel 1, better represents linear elements such as rivers. Consequently, manual editing and adaptation of the reference data were necessary to align the selected maps with the spatial resolution of

the images and to correct certain areas of the map. The adaptation process relied on the visual interpretation conducted by experts.

**Table 1.** Land cover maps used and their accuracies compared to the respective annotated ground truth.

Product	Accuracy	F1_Score
Google_2019	0.56	0.56
Esri_2019	0.59	0.56
Esa_2020	0.61	0.60
Glad_2019	0.69	0.67
Talandcover map	0.75	0.76

Each image section in the dataset comes with a corresponding mask, which is a matrix with values ranging from 0 to 5. These values indicate the index of land cover class (see Figure 7).

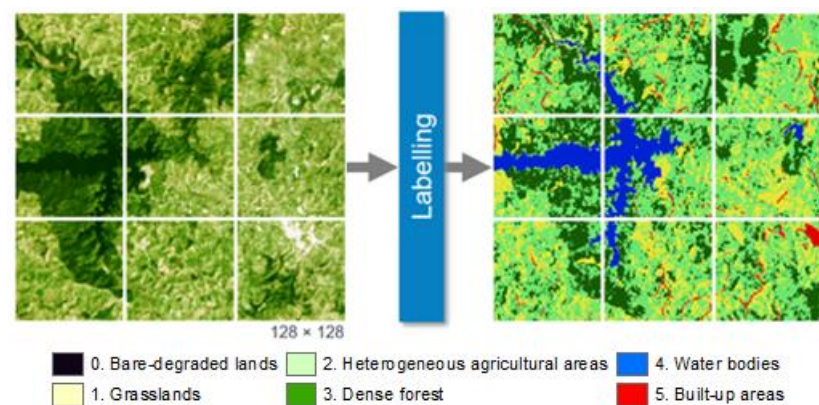


**Figure 7.** The Association of Masks to Image Sections in the Dataset.

The representation of land cover for the geographical area considered in the construction of the dataset is as follows:

- Bare-degraded lands: 0.61%
- Dense forest: 48.65%
- Heterogeneous agricultural areas: 22.66%
- Grasslands: 25.8%
- Water bodies: 1.09%
- Built-up areas: 1.20%

#### 4.2. Balanced Dataset

The balanced selection of the image set was facilitated through the utilization of a Python script that incorporated the GDAL and OGR libraries, and the script produced a sliding window of dimensions  $128 \times 128$  that was georeferenced and applied to scan the tiles or image mosaics. The spatial frames that met a predetermined minimum threshold of the selected coverage were retained, while those that displayed overlap were discarded.

The spatial frames that were chosen were utilized to extract the pixel values from the satellite images and their corresponding labels. The determination of image sections for each class was based on their representativeness. This suggests that, of all the images examined, only those that met the established criteria of containing either 50% or 70% of pixels corresponding to a particular class were selected. After this filtering, an excess of spatial frames from the dominant cover were found, and these arise from the imbalance observed in the data. To counteract this imbalance, the number of images from the least represented class was used as a benchmark to determine the quantity of images for each

class in the training dataset. For the 50% and 70% thresholds, 234 and 122 images were selected per class, respectively (see Table 2). During the review process, image sections that displayed a singular value across all pixels were discarded. Ultimately, employing an 80/20 split for training and testing, a total of 1389 and 731 images were utilized for the 50% and 70% thresholds, respectively.

**Table 2.** Quantity of image sections that comply with a minimum presence percentage by coverage, i.e., 50% and 70%.

Coverage Type	50%	70%
Bare-degraded lands	234	122
Grasslands	22,515	10,228
Heterogeneous agricultural areas	26,225	7414
Dense forest	61,610	45,617
Bodies of water	670	343
Built-up areas	1004	689
Training	1111	584
Test	278	147
Total	1389	731

Table 3 present pixel distribution for random samples, 50% balanced samples, and 70% balanced samples. The random sample model had 4000 training and 1000 test images, the 50% sample model had 1111 training and 278 test images, while the 70% sample model used 584 training and 147 test images.

**Table 3.** Comparison of sampled pixel distribution for different land classes across the three sampling models.

Class		Random Sample		50% Sample		70% Sample	
		Training	Test	Training	Test	Training	Test
Bare-degraded lands	px	345,589	67,380	1,815,872	700,986	1,228,192	308,143
	%	0.53%	0.41%	9.98%	15.39%	12.84%	12.79%
Grasslands	px	14,648,492	3,825,272	4,300,293	1,135,534	2,049,492	484,262
	%	22.35%	23.35%	23.62%	24.93%	21.42%	20.11%
Heterogeneous agricultural areas	px	15,655,124	3,831,559	3,751,735	842,770	1,819,210	419,836
	%	23.89%	23.39%	20.61%	18.50%	19.01%	17.43%
Dense forest	px	33,541,637	8,318,905	4,055,664	883,921	1,794,289	525,788
	%	51.18%	50.77%	22.28%	19.41%	18.75%	21.83%
Bodies of water	px	264,911	105,181	1,988,487	545,079	1,293,598	332,603
	%	0.40%	0.64%	10.92%	11.97%	13.52%	13.81%
Built-up areas	px	1,080,247	235,703	2,290,573	446,462	1,383,475	337,816
	%	1.65%	1.44%	12.58%	9.80%	14.46%	14.03%

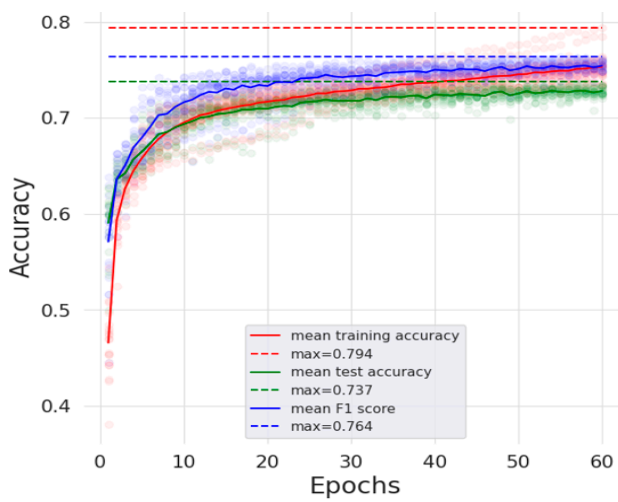
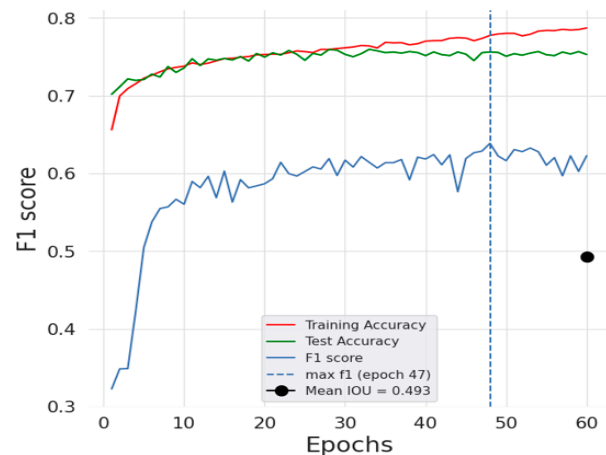
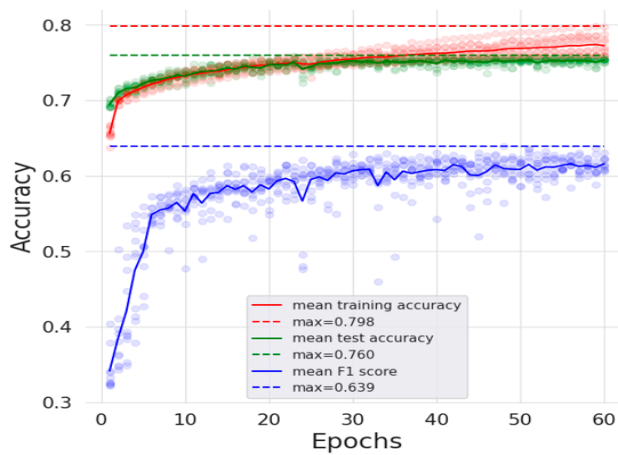
#### 4.3. Model Training

Given the imbalance of classes and to assess learning trends, ten models per epoch were executed. Each model was trained using Google Colab to take advantage of the T4 GPU execution environment.

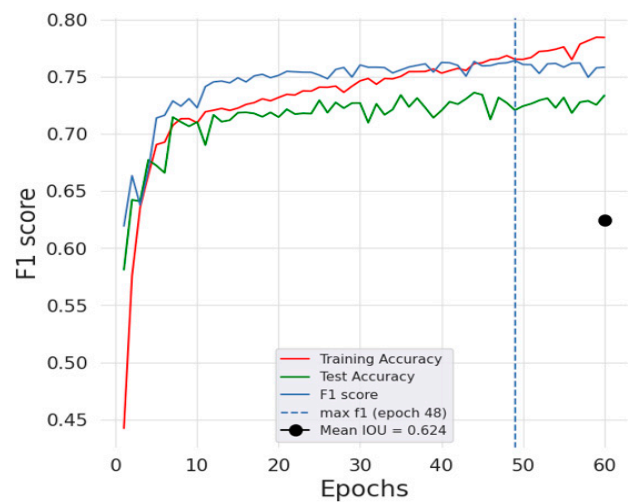
The training parameters for each model are listed below in Table 4. We present the results of the models trained with each dataset: random samples and balanced samples at both 50% and 70%. For each epoch, the results of the ten models were plotted to identify learning patterns over its respective test set (see Figure 8) and the confusion matrix for the best model for each sampling strategy is shown in Figure 9.

**Table 4.** General parameters list for the training process.

Parameter	Value
Input Channels	NIR (Near-Infrared), R (Red), G (Green)
Epochs	60
Batch Size	16
Optimization Function	Adam (Adaptive Moment Optimization)
Beta_1	0.9
Beta_2	0.999
Epsilon	$1 \times 10^{-7}$
Loss Function	Sparse Categorical Cross Entropy
Learning Rate	0.001
Regularization Method	Dropout rate 0.5



(a)



(b)

**Figure 8.** Cont.

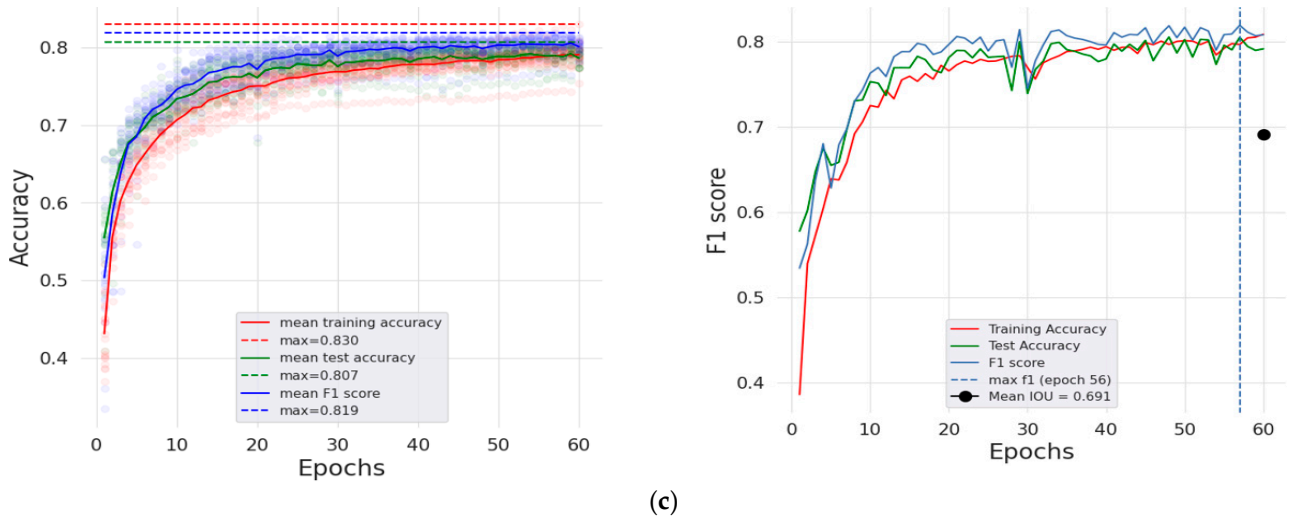


**Figure 8.** (Left) Metrics for the set of models trained and (right) metrics for the best model found for (a) random sample, (b) sample of 50%, and (c) sample of 70%.

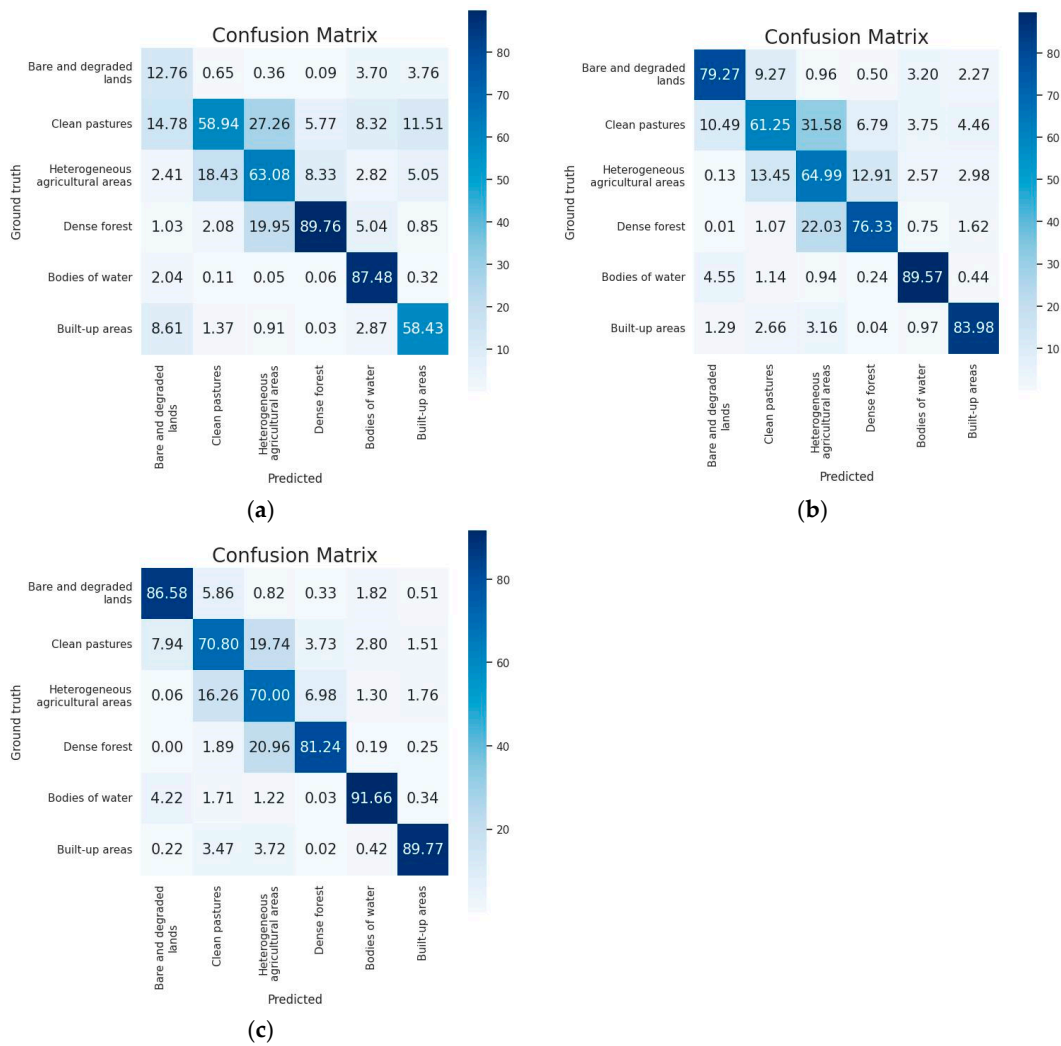


**Figure 9.** Confusion matrix for the (a) random sample, (b) sample of 50%, and (c) sample of 70%.

The three datasets are openly available at the following link <https://zenodo.org/record/8219553> (accessed on 2 November 2023).

In the context of the presented models, the prediction was carried out for a specific set of images to conduct a visual comparative analysis of the results. Several examples are illustrated in Figure 10. It is noteworthy that the models exhibiting the highest F1 score were taken into consideration for this examination.

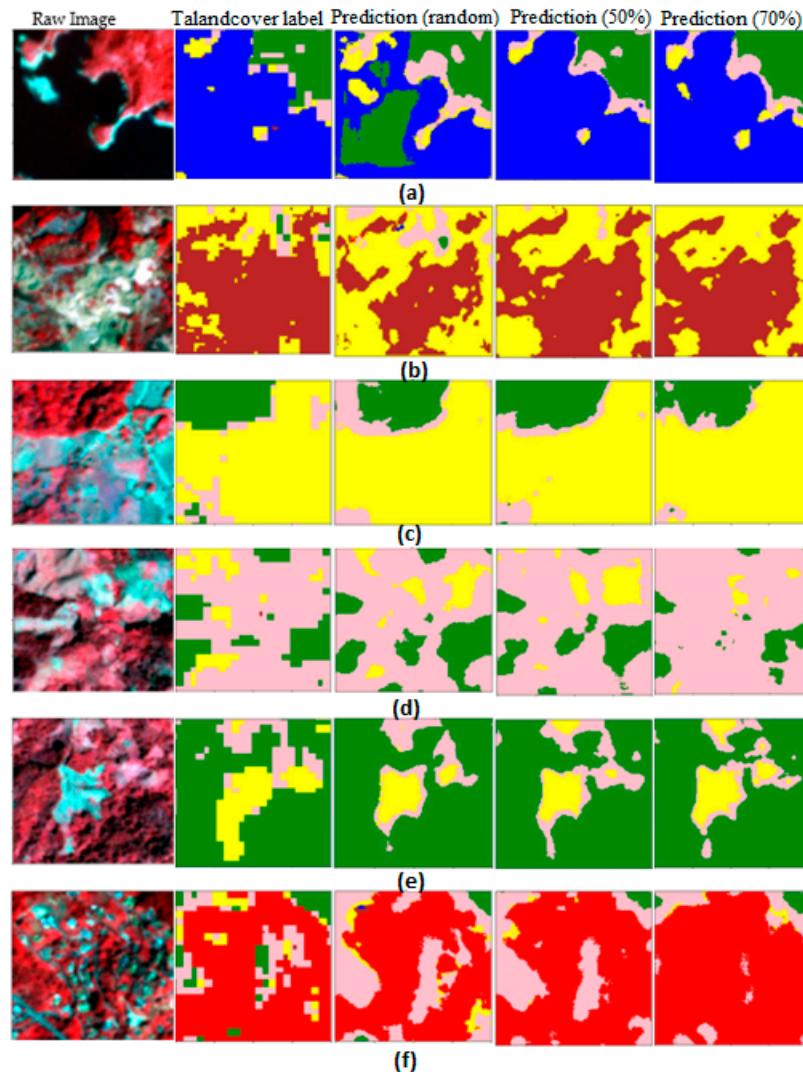


**Figure 10.** Results Examples from Three Prediction Models. From left to right: real image, base label, predictions with random selection, 50% threshold, and 70% threshold. Subfigures a–f are representative images of each type of coverage (a) water bodies: Blue, (b) bare-degraded lands: Brown, (c) grasslands: Yellow, (d) agricultural heterogeneous areas: Pink (e), dense forest: Green, (f) built-up Areas: Red.

The model trained on a random sample exhibited certain challenges in segmentation, as evident in Figure 10a. In this image, forest areas were erroneously identified in regions that should correspond to bodies of water. This discrepancy can be attributed to the bias present in the training sample, leading to misclassifications and an overestimation of dense forest coverage.

Furthermore, the models trained on balanced samples of 50% and 70% demonstrated superior performance in predicting the less representative classes, such as bare-degraded lands (e.g., Figure 10b), as well as built-up areas. These coverages were delineated with higher precision compared to the model trained on a random sample.

Despite the low representativeness of bodies of water in the samples, all three models achieved high prediction values for this class. This phenomenon can be explained by the fact that the spectral characteristics of bodies of water are highly homogeneous and distinct from other classes, thereby facilitating their accurate segmentation and prediction in the models.

Although global maps are a valuable contribution to monitoring coverage and a starting point for having a large amount of training data, it is important to consider that ML methods were used to build these global maps and that ML algorithms can generate biases in their results that could be reproduced by the methods trained on their data.

On the other hand, the accuracy of the models was evaluated on their respective test set. Consequently, the results cannot be used to compare due to the differences in the dataset's composition. Therefore, as a comparison criterion, the accuracy of the models trained with the TALANDCOVER label was evaluated on the same data delimited by an expert (ground truth), which is considered closer to the geographic reality of the study area, obtaining F1 score values of 0.70, 0.72, and 0.74 for the random model, balanced 50%, and balanced 70%, respectively. Figure 11 shows some examples of the results.

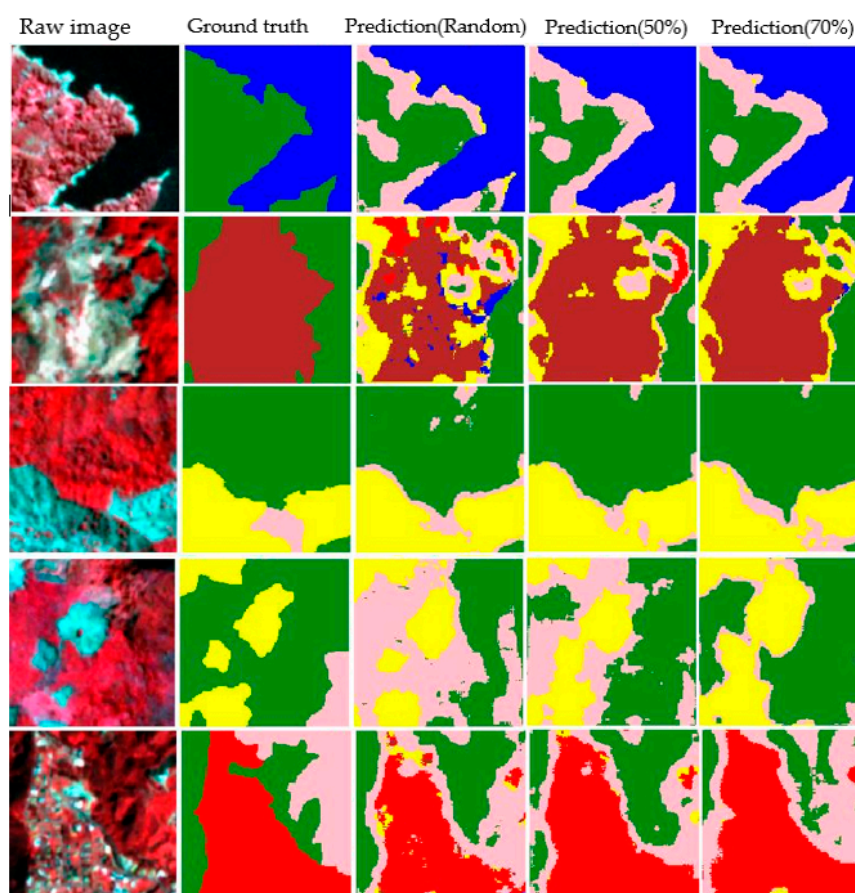


**Figure 11.** Results Examples from Three Prediction Models. From left to right: real image, ground truth, predictions with random selection, 50% threshold, and 70% threshold. The color key: Blue: water bodies, Pink: agricultural heterogeneous areas, Yellow: grasslands, Red: built-up areas, Brown: bare-degraded Lands.

## 5. Discussion

To illustrate the utilization of the diverse datasets suggested in this investigation, U-net models were trained on each respective set. A sampling strategy was employed to tackle the issue of class imbalance, wherein the minimum percentage per class was utilized. The U-Net model achieved relatively high accuracy after 20 epochs, with gradual improvement thereafter and fluctuations in the curves becoming more stable in later epochs. The results

indicated that the datasets with 50% and 70% facilitated a greater degree of learning. The experimental outcomes indicate that the 70% sample yielded the most precise results over ground truth constructed by expert knowledge with an F1 score of 0.74 and performance in terms of accuracy (0.80) and F1 score (0.819) on its own test data.

In situations where the training set is restricted, such as in the 70% sample, models tend to exhibit overfitting. The experimental results indicate that there was no observed evidence of overfitting in the metric curves of the ten models that were executed. The observed phenomenon can be attributed to the implementation of dropout methodologies [91] and the utilization of an equitable sample, which prevents the dominance of the most prevalent category from influencing the learning process.

Despite the limited size of balanced sample sets, the utilization of high-quality data or a well-designed sampling strategy can substantially mitigate the training time and computational load. Furthermore, the proposed sampling techniques aim to optimally utilize the available original information and provide additional instances for the underrepresented categories, thus laying a foundation for data augmentation, a method commonly utilized in the realm of machine learning to enhance the generalization capabilities of algorithms [1].

The results are relative to the comparisons made in relation to the type of images used and the LULCC classification system. Subsequent investigations might facilitate understanding of the variations in accuracy across different datasets, LULCC frameworks, and supervised classification algorithms that utilize loss functions, such as focal loss, IoU loss, or diverse hyperparameter configurations. As posited by [92], architectures that encompass a higher number of filters or layers can discern intricate patterns with increased precision.

The predominant source of ambiguity was identified within agricultural zones, potentially due to the heterogeneous spectral responses of mixed-cover agricultural terrains inclusive of trees, herbs, and shrubs. Another challenge lies in distinguishing between plantations and forests as these two covers present significant differences in their biodiversity and their ability to provide ecosystem services. The purview of this study does not include discerning between these two cover categories as the spectral characteristics of the data are constrained and fail to address the spectral similarity of the various components [62]. Nonetheless, to improve the discrimination between diverse land cover categories, the bands in the proposed dataset could be complemented with radar imagery [49,63,65] or additional spectral bands from other sensors like Sentinel-2 [62].

The variability within a given class of a sample that is derived from a geographically extensive region may have an impact on the process of model learning. As an example, it is possible for semantic categories like highland forests and floodplain forests to exhibit varying spectral signatures depending on their respective locations. Future investigations might incorporate the suggested balanced sampling approach, along with stratified sampling based on continuous geographical regions or eco-climate, as proposed by [53].

We believe that the approach taken in this research to evaluate different models presents a more pragmatic perspective on the prospective applications of the proposed dataset, while also functioning as a reference for the instruction and/or development of novel architectures.

### 5.1. Dataset Generation

The TALANDCOVER dataset (see Table 5) obtained from NICFI satellite imagery includes a categorical mask with values from 0 to 5 that represents six classes.

**Table 5.** TALANDCOVER Satellite Imagery Dataset Details.

Item	Description
Application field	Satellite image segmentation
Type of Data collected	NICFI satellite images: planet_medres_normalized_analytic_2018-12_2019-05_mosaic
GIS Software Used	QGIS <sup>1</sup> V3.22.2
Scripting Language for Data Processing and Products	Python 3.8
Packages Used in Programming Language	GDAL <sup>2</sup> , OGR <sup>3</sup>
Collection Year	2019
Number of Classes	6
Type of Segmented Data	Multiclass mask
Dataset Size	747.8 MB (.zip)
Image Format	Tif
Number of Images	1389 (balanced-50%)-731 (balanced-70%)-5000 (random)
Rows and Columns	128 × 128
Spectral Resolution of Images	4 bands, R-G-B-NIR
Radiometric Resolution of Images	16 bit

<sup>1</sup> QGIS (Quantum Geographic Information System). <sup>2</sup> GDAL (Geospatial Data Abstraction Library). <sup>3</sup> OGR (OpenGIS Simple Features Reference Implementation).

0. Bare-degraded land
1. Grasslands
2. Agricultural heterogeneous areas
3. Dense forest
4. Water bodies
5. Built-up areas

### 5.2. Practical Application of the Dataset

The proposed dataset offers practical applications for understanding and addressing various socio-economic and environmental challenges. By detecting and classifying different types of land cover in highly transformed landscapes, this dataset enables comprehensive studies on critical topics, such as food security, urban growth, deforestation, and climate change.

One significant practical implication of this dataset is its ability to support research on food production systems, particularly in terms of security and stability. By identifying heterogeneous landscapes, this dataset enables monitor land use patterns, and the impact of agricultural practices on the environment.

Furthermore, the dataset contributes to efforts in combating deforestation and preserving forest ecosystems. By accurately delineating dense forest areas and monitoring changes to their extent, it enables the assessment of deforestation rates, habitat loss, and biodiversity conservation. This information is crucial for designing effective conservation strategies, promoting reforestation initiatives, and addressing climate change impacts.

On the other hand, given the different methodological approaches existing in the literature, the proposed datasets (random, balanced) yield the training of different deep learning models and perform comparisons to establish general conclusions regarding the strengths and weaknesses of an implementation.

## 6. Conclusions

The effective monitoring of LULCC in the tropical Andes region presents challenges due the mountainous topography and the long history of anthropic transformation. Several datasets for training DL models have been proposed in the literature. However, these datasets have predominantly been constructed in urban contexts and high-latitude areas. To improve the application of DL models, primarily in the tropical region, the TALAND-

COVER dataset was developed. In this paper, we explained the preprocessing of the satellite images and the construction of the datasets with different sampling strategies and we present the prediction of several models with their metrics to provide some baselines for the use of the data.

The methodology presents an efficient workflow to generate a large amount of labeled data without performing this task 100% manually, taking advantage of existing coverage datasets. Although these data individually have problems, particularly as they are developed into global extensions, the joint use of these products provides a useful foundation for collecting large amounts of training data.

Creating the TALANDCOVER dataset for the geographic area of Antioquia, Colombia contributes to the field of land cover classification. The dataset is made up of multiband R-G-B-NIR pictures and matching multiclass labels, and it may be used for training, validation, and testing. The dataset, which has a spatial resolution of more than 10 m, allows researchers to study land cover changes patterns, and the effects of human activities on the environment in the tropical area. The collection also helps climate change research by examining the relationships between land cover cycles and climatic processes.

The set of models trained with the different datasets and using the U-Net architecture allowed us to observe the learning capabilities not only on the test data but also on the dataset built manually by an expert. This represents a guide and starting point for the construction of new models where greater computational efficiency and greater precision in their generalization capacity are sought.

**Author Contributions:** Conceptualization, L.F.G.-O.; methodology, L.F.G.-O., G.S.-T. and J.W.B.-B.; software, L.F.G.-O.; validation, G.S.-T. and J.W.B.-B.; formal analysis, L.F.G.-O.; investigation, L.F.G.-O., G.S.-T. and J.W.B.-B.; data curation, L.F.G.-O.; writing—original draft preparation, L.F.G.-O. and G.S.-T.; writing—review and editing, L.F.G.-O., G.S.-T. and J.W.B.-B.; visualization, L.F.G.-O.; supervision, G.S.-T. and J.W.B.-B.; funding acquisition, J.W.B.-B. All authors have read and agreed to the published version of the manuscript.

**Funding:** This research received no external funding.

**Institutional Review Board Statement:** Not applicable.

**Informed Consent Statement:** Not applicable.

**Data Availability Statement:** The data presented in this study are openly available in Zenodo at <https://zenodo.org/record/8219553> (accessed on 2 November 2023).

**Acknowledgments:** We would like to thank GIDIA (Research group in Artificial Intelligence of the Universidad Nacional de Colombia) for providing guidelines, reviews to the work, and use of facilities.

**Conflicts of Interest:** The authors declare no conflict of interest. The funders had no role in the design of the study; in the collection, analyses, or interpretation of data; in the writing of the manuscript; or in the decision to publish the results.

## References

1. Lalitha, V.; Latha, B. A Review on Remote Sensing Imagery Augmentation Using Deep Learning. *Mater. Today Proc.* **2022**, *62*, 4772–4778. [[CrossRef](#)]
2. Yuan, X.; Shi, J.; Gu, L. A Review of Deep Learning Methods for Semantic Segmentation of Remote Sensing Imagery. *Expert Syst. Appl.* **2021**, *169*, 114417. [[CrossRef](#)]
3. Singh, S.; Reddy, C.S.; Pasha, S.V.; Dutta, K.; Saranya, K.R.L.; Satish, K.V. Modeling the Spatial Dynamics of Deforestation and Fragmentation Using Multi-Layer Perceptron Neural Network and Landscape Fragmentation Tool. *Ecol. Eng.* **2017**, *99*, 543–551. [[CrossRef](#)]
4. Zhang, B.; Li, W.; Zhang, C. Analyzing Land Use and Land Cover Change Patterns and Population Dynamics of Fast-Growing US Cities: Evidence from Collin County, Texas. *Remote Sens. Appl. Soc. Environ.* **2022**, *27*, 100804. [[CrossRef](#)]
5. Darem, A.A.; Alhashmi, A.A.; Almadani, A.M.; Alanazi, A.K.; Sutantra, G.A. Development of a Map for Land Use and Land Cover Classification of the Northern Border Region Using Remote Sensing and GIS. *Egypt. J. Remote Sens. Space Sci.* **2023**, *26*, 341–350. [[CrossRef](#)]

6. Hosseiny, B.; Abdi, A.M.; Jamali, S. Urban Land Use and Land Cover Classification with Interpretable Machine Learning—A Case Study Using Sentinel-2 and Auxiliary Data. *Remote Sens. Appl. Soc. Environ.* **2022**, *28*, 100843. [CrossRef]
7. Parente, L.; Taquary, E.; Silva, A.P.; Souza, C.; Ferreira, L. Next Generation Mapping: Combining Deep Learning, Cloud Computing, and Big Remote Sensing Data. *Remote Sens.* **2019**, *11*, 2881. [CrossRef]
8. Hermosilla, T.; Wulder, M.A.; White, J.C.; Coops, N.C. Land Cover Classification in an Era of Big and Open Data: Optimizing Localized Implementation and Training Data Selection to Improve Mapping Outcomes. *Remote Sens. Environ.* **2022**, *268*, 112780. [CrossRef]
9. Anderson, K.; Ryan, B.; Sonntag, W.; Kavvada, A.; Friedl, L. Earth Observation in Service of the 2030 Agenda for Sustainable Development. *Geo-Spat. Inf. Sci.* **2017**, *20*, 77–96. [CrossRef]
10. Holloway, J.; Mengersen, K. Statistical Machine Learning Methods and Remote Sensing for Sustainable Development Goals: A Review. *Remote Sens.* **2018**, *10*, 1365. [CrossRef]
11. Helber, P.; Bischke, B.; Dengel, A.; Borth, D. EuroSAT: A Novel Dataset and Deep Learning Benchmark for Land Use and Land Cover Classification. *IEEE J. Sel. Top. Appl. Earth Obs. Remote Sens.* **2019**, *12*, 2217–2226. [CrossRef]
12. Ma, L.; Liu, Y.; Zhang, X.; Ye, Y.; Yin, G.; Johnson, B.A. Deep Learning in Remote Sensing Applications: A Meta-Analysis and Review. *ISPRS J. Photogramm. Remote Sens.* **2019**, *152*, 166–177. [CrossRef]
13. Potsdam, I. 2D Semantic Labeling Contest—Potsdam 2019. ISPRS Potsdam 2D Semantic Labeling Dataset. Available online: <https://www.isprs.org/education/benchmarks/UrbanSemLab/2d-sem-label-potsdam.aspx> (accessed on 24 June 2023).
14. Báez, S.; Jaramillo, L.; Cuesta, F.; Donoso, D.A. Effects of Climate Change on Andean Biodiversity: A Synthesis of Studies Published until 2015. *Neotrop. Biodivers.* **2016**, *2*, 181–194. [CrossRef]
15. Zalles, V.; Hansen, M.C.; Potapov, P.V.; Parker, D.; Stehman, S.V.; Pickens, A.H.; Parente, L.L.; Ferreira, L.G.; Song, X.-P.; Hernandez-Serna, A.; et al. Rapid Expansion of Human Impact on Natural Land in South America since 1985. *Sci. Adv.* **2021**, *7*, eabg1620. [CrossRef] [PubMed]
16. Pérez-Escobar, O.A.; Zizka, A.; Bermúdez, M.A.; Meseguer, A.S.; Condamine, F.L.; Hoorn, C.; Hooghiemstra, H.; Pu, Y.; Bogarín, D.; Boschman, L.M.; et al. The Andes through Time: Evolution and Distribution of Andean Floras. *Trends Plant Sci.* **2022**, *27*, 364–378. [CrossRef]
17. Schmitt, M.; Hughes, L.H.; Qiu, C.; Zhu, X.X. SEN12MS—A Curated Dataset of Georeferenced Multi-Spectral Sentinel-1/2 Imagery for Deep Learning and Data Fusion. *arXiv* **2019**, arXiv:1906.07789. [CrossRef]
18. Sumbul, G.; Charfuelan, M.; Demir, B.; Markl, V. Bigearthnet: A Large-Scale Benchmark Archive for Remote Sensing Image Understanding. In Proceedings of the IGARSS 2019—2019 IEEE International Geoscience and Remote Sensing Symposium 2019, Yokohama, Japan, 28 July–2 August 2019; pp. 5901–5904.
19. Qi, X.; Zhu, P.; Wang, Y.; Zhang, L.; Peng, J.; Wu, M.; Chen, J.; Zhao, X.; Zang, N.; Mathiopoulos, P.T. MLRSNet: A Multi-Label High Spatial Resolution Remote Sensing Dataset for Semantic Scene Understanding. *arXiv* **2020**, arXiv:2010.00243. [CrossRef]
20. Zhu, Q.; Deng, W.; Zheng, Z.; Zhong, Y.; Guan, Q.; Lin, W.; Zhang, L.; Li, D. A Spectral-Spatial-Dependent Global Learning Framework for Insufficient and Imbalanced Hyperspectral Image Classification. *IEEE Trans. Cybern.* **2022**, *52*, 11709–11723. [CrossRef]
21. Mao, L.; Zheng, Z.; Meng, X.; Zhou, Y.; Zhao, P.; Yang, Z.; Long, Y. Large-Scale Automatic Identification of Urban Vacant Land Using Semantic Segmentation of High-Resolution Remote Sensing Images. *Landsc. Urban Plan.* **2022**, *222*, 104384. [CrossRef]
22. Yeung, H.W.F.; Zhou, M.; Chung, Y.Y.; Moule, G.; Thompson, W.; Ouyang, W.; Cai, W.; Bennamoun, M. Deep-Learning-Based Solution for Data Deficient Satellite Image Segmentation. *Expert Syst. Appl.* **2022**, *191*, 116210. [CrossRef]
23. ISPRS Vaihingen 2D Semantic Labeling Dataset. Available online: <https://www.isprs.org/education/benchmarks/UrbanSemLab/2d-sem-label-vaihingen.aspx> (accessed on 24 June 2023).
24. Van Etten, A. Satellite Imagery Multiscale Rapid Detection with Windowed Networks. In Proceedings of the 2019 IEEE Winter Conference on Applications of Computer Vision (WACV), Waikoloa, HI, USA, 7–11 January 2019; pp. 735–743.
25. Toker, A.; Kondmann, L.; Weber, M.; Eisenberger, M.; Camero, A.; Hu, J.; Hoderlein, A.P.; Şenaras, Ç.; Davis, T.; Cremers, D.; et al. DynamicEarthNet: Daily Multi-Spectral Satellite Dataset for Semantic Change Segmentation. In Proceedings of the 2022 IEEE/CVF Conference on Computer Vision and Pattern Recognition (CVPR), New Orleans, LA, USA, 18–24 June 2022; pp. 21126–21135.
26. Brown, C.F.; Brumby, S.P.; Guzder-Williams, B.; Birch, T.; Hyde, S.B.; Mazzariello, J.; Czerwinski, W.; Pasquarella, V.J.; Haertel, R.; Ilyushchenko, S.; et al. Dynamic World, Near Real-Time Global 10 m Land Use Land Cover Mapping. *Sci. Data* **2022**, *9*, 251. [CrossRef]
27. Zanaga, D.; Van De Kerchove, R.; De Keersmaecker, W.; Souverijns, N.; Brockmann, C.; Quast, R.; Wevers, J.; Grosu, A.; Paccini, A.; Vergnaud, S.; et al. ESA WorldCover 10 m 2020 V100. *Zenodo* **2021**.
28. Bragagnolo, L.; da Silva, R.V.; Grzybowski, J.M.V. Amazon and Atlantic Forest Image Datasets for Semantic Segmentation. *Zenodo* **2021**. [CrossRef]
29. De Moreno, G.M.S.; de Júnior, O.A.C.; de Carvalho, O.L.F.; Andrade, T.C. Deep Semantic Segmentation of Mangroves in Brazil Combining Spatial, Temporal, and Polarization Data from Sentinel-1 Time Series. *Ocean Coast. Manag.* **2023**, *231*, 106381. [CrossRef]
30. Edgeworth, F.Y. On the Probable Errors of Frequency-Constants (Contd.). *J. R. Stat. Soc.* **1908**, *71*, 499–512. [CrossRef]

31. Shivakumar, B.R.; Rajashekararadhya, S.V. Investigation on Land Cover Mapping Capability of Maximum Likelihood Classifier: A Case Study on North Canara, India. *Procedia Comput. Sci.* **2018**, *143*, 579–586. [[CrossRef](#)]
32. Mollick, T.; Azam, M.G.; Karim, S. Geospatial-Based Machine Learning Techniques for Land Use and Land Cover Mapping Using a High-Resolution Unmanned Aerial Vehicle Image. *Remote Sens. Appl. Soc. Environ.* **2023**, *29*, 100859. [[CrossRef](#)]
33. Sam, S.C.; Balasubramanian, G. Spatiotemporal Detection of Land Use/Land Cover Changes and Land Surface Temperature Using Landsat and MODIS Data across the Coastal Kanyakumari District, India. *Geod. Geodyn.* **2023**, *14*, 172–181. [[CrossRef](#)]
34. Otukei, J.R.; Blaschke, T. Land Cover Change Assessment Using Decision Trees, Support Vector Machines and Maximum Likelihood Classification Algorithms. *Int. J. Appl. Earth Obs. Geoinf.* **2010**, *12*, S27–S31. [[CrossRef](#)]
35. Saha, S.; Saha, M.; Mukherjee, K.; Arabameri, A.; Ngo, P.T.T.; Paul, G.C. Predicting the Deforestation Probability Using the Binary Logistic Regression, Random Forest, Ensemble Rotational Forest, REPTree: A Case Study at the Gumani River Basin, India. *Sci. Total Environ.* **2020**, *730*, 139197. [[CrossRef](#)]
36. Mangkhaseum, S.; Hanazawa, A. Comparison of Machine Learning Classifiers for Land Cover Changes Using Google Earth Engine. In Proceedings of the 2021 IEEE International Conference on Aerospace Electronics and Remote Sensing Technology (ICARES), Bali, Indonesia, 3–4 November 2021; pp. 1–7.
37. Garg, R.; Kumar, A.; Bansal, N.; Prateek, M.; Kumar, S. Semantic Segmentation of PolSAR Image Data Using Advanced Deep Learning Model. *Sci. Rep.* **2021**, *11*, 15365. [[CrossRef](#)]
38. Palanisamy, P.A.; Jain, K.; Bonafoni, S. Machine Learning Classifier Evaluation for Different Input Combinations: A Case Study with Landsat 9 and Sentinel-2 Data. *Remote Sens.* **2023**, *15*, 3241. [[CrossRef](#)]
39. Yuh, Y.G.; Tracz, W.; Matthews, H.D.; Turner, S.E. Application of Machine Learning Approaches for Land Cover Monitoring in Northern Cameroon. *Ecol. Inform.* **2023**, *74*, 101955. [[CrossRef](#)]
40. Breiman, L. Random Forests. *Mach. Learn.* **2001**, *45*, 5–32. [[CrossRef](#)]
41. Valle, T.M.D.; Jiang, P. Comparison of Common Classification Strategies for Large-Scale Vegetation Mapping over the Google Earth Engine Platform. *Int. J. Appl. Earth Obs. Geoinf.* **2022**, *115*, 103092. [[CrossRef](#)]
42. Zhang, F.; Yang, X. Improving Land Cover Classification in an Urbanized Coastal Area by Random Forests: The Role of Variable Selection. *Remote Sens. Environ.* **2020**, *251*, 112105. [[CrossRef](#)]
43. Wu, H.; Lin, A.; Xing, X.; Song, D.; Li, Y. Identifying Core Driving Factors of Urban Land Use Change from Global Land Cover Products and POI Data Using the Random Forest Method. *Int. J. Appl. Earth Obs. Geoinf.* **2021**, *103*, 102475. [[CrossRef](#)]
44. Amorim, F.d.L.L.d.; Rick, J.; Lohmann, G.; Wiltshire, K.H. Evaluation of Machine Learning Predictions of a Highly Resolved Time Series of Chlorophyll-a Concentration. *Appl. Sci.* **2021**, *11*, 7208. [[CrossRef](#)]
45. Yang, H.L.; Yuan, J.; Lunga, D.; Laverdiere, M.; Rose, A.; Bhaduri, B. Building Extraction at Scale Using Convolutional Neural Network: Mapping of the United States. *IEEE J. Sel. Top. Appl. Earth Obs. Remote Sens.* **2018**, *11*, 2600–2614. [[CrossRef](#)]
46. Ienco, D.; Gaetano, R.; Dupaquier, C.; Maurel, P. Land Cover Classification via Multitemporal Spatial Data by Deep Recurrent Neural Networks. *IEEE Geosci. Remote Sens. Lett.* **2017**, *14*, 1685–1689. [[CrossRef](#)]
47. Lan, R.; Li, Z.; Liu, Z.; Gu, T.; Luo, X. Hyperspectral Image Classification Using K-Sparse Denoising Autoencoder and Spectral-Restricted Spatial Characteristics. *Appl. Soft Comput.* **2019**, *74*, 693–708. [[CrossRef](#)]
48. LeCun, Y.; Bengio, Y.; Hinton, G. Deep Learning. *Nature* **2015**, *521*, 436–444. [[CrossRef](#)] [[PubMed](#)]
49. Solórzano, J.V.; Mas, J.F.; Gao, Y.; Gallardo-Cruz, J.A. Land Use Land Cover Classification with U-Net: Advantages of Combining Sentinel-1 and Sentinel-2 Imagery. *Remote Sens.* **2021**, *13*, 3600. [[CrossRef](#)]
50. Remeberger, O.; Fischer, P.; Brox, T. U-Net: Convolutional Networks for Biomedical Image Segmentation. In *Proceedings of the Medical Image Computing and Computer-Assisted Intervention—MICCAI 2015*; Navab, N., Hornegger, J., Wells, W.M., Frangi, A.F., Eds.; Springer International Publishing: Cham, Switzerland, 2015; pp. 234–241.
51. Flood, N.; Watson, F.; Collett, L. Using a U-Net Convolutional Neural Network to Map Woody Vegetation Extent from High Resolution Satellite Imagery across Queensland, Australia. *Int. J. Appl. Earth Obs. Geoinf.* **2019**, *82*, 101897. [[CrossRef](#)]
52. Mazza, A.; Sica, F.; Rizzoli, P.; Scarpa, G. TanDEM-X Forest Mapping Using Convolutional Neural Networks. *Remote Sens.* **2019**, *11*, 2980. [[CrossRef](#)]
53. Stoian, A.; Poulain, V.; Inglada, J.; Poughon, V.; Derksen, D. Land Cover Maps Production with High Resolution Satellite Image Time Series and Convolutional Neural Networks: Adaptations and Limits for Operational Systems. *Remote Sens.* **2019**, *11*, 1986. [[CrossRef](#)]
54. Caraballo-Vega, J.A.; Carroll, M.L.; Neigh, C.S.R.; Wooten, M.; Lee, B.; Weis, A.; Aronne, M.; Alemu, W.G.; Williams, Z. Optimizing WorldView-2, -3 Cloud Masking Using Machine Learning Approaches. *Remote Sens. Environ.* **2023**, *284*, 113332. [[CrossRef](#)]
55. Wang, X.; Jing, S.; Dai, H.; Shi, A. High-Resolution Remote Sensing Images Semantic Segmentation Using Improved UNet and SegNet. *Comput. Electr. Eng.* **2023**, *108*, 108734. [[CrossRef](#)]
56. Wagner, F.H.; Dalagnol, R.; Tagle Casapia, X.; Streher, A.S.; Phillips, O.L.; Gloor, E.; Aragão, L.E.O.C. Regional Mapping and Spatial Distribution Analysis of Canopy Palms in an Amazon Forest Using Deep Learning and VHR Images. *Remote Sens.* **2020**, *12*, 2225. [[CrossRef](#)]
57. Giang, T.L.; Dang, K.B.; Toan Le, Q.; Nguyen, V.G.; Tong, S.S.; Pham, V.-M. U-Net Convolutional Networks for Mining Land Cover Classification Based on High-Resolution UAV Imagery. *IEEE Access* **2020**, *8*, 186257–186273. [[CrossRef](#)]
58. Du, L.; McCarty, G.W.; Zhang, X.; Lang, M.W.; Vanderhoof, M.K.; Li, X.; Huang, C.; Lee, S.; Zou, Z. Mapping Forested Wetland Inundation in the Delmarva Peninsula, USA Using Deep Convolutional Neural Networks. *Remote Sens.* **2020**, *12*, 644. [[CrossRef](#)]

59. Alzubaidi, L.; Zhang, J.; Humaidi, A.J.; Al-Dujaili, A.; Duan, Y.; Al-Shamma, O.; Santamaría, J.; Fadhel, M.A.; Al-Amidie, M.; Farhan, L. Review of Deep Learning: Concepts, CNN Architectures, Challenges, Applications, Future Directions. *J. Big Data* **2021**, *8*, 53. [[CrossRef](#)] [[PubMed](#)]
60. Xie, Q.; Dai, Z.; Hovy, E.; Luong, M.-T.; Le, Q.V. Unsupervised Data Augmentation for Consistency Training. *arXiv* **2020**, arXiv:1904.12848.
61. Cubuk, E.D.; Zoph, B.; Mane, D.; Vasudevan, V.; Le, Q.V. AutoAugment: Learning Augmentation Policies from Data. *arXiv* **2019**, arXiv:1805.09501.
62. Awuah, K.T.; Aplin, P. Fusion of Sentinel-2 Data with High Resolution Open Access Planet Basemaps for Grazing Lawn Detection in Southern African Savannas. In Proceedings of the 2021 IEEE International Geoscience and Remote Sensing Symposium IGARSS, Brussels, Belgium, 11–16 July 2021; pp. 1409–1412.
63. Vizzari, M. PlanetScope, Sentinel-2, and Sentinel-1 Data Integration for Object-Based Land Cover Classification in Google Earth Engine. *Remote Sens.* **2022**, *14*, 2628. [[CrossRef](#)]
64. Prasad, P.; Loveson, V.J.; Chandra, P.; Kotha, M. Evaluation and Comparison of the Earth Observing Sensors in Land Cover/Land Use Studies Using Machine Learning Algorithms. *Ecol. Inform.* **2022**, *68*, 101522. [[CrossRef](#)]
65. Heckel, K.; Urban, M.; Schratz, P.; Mahecha, M.D.; Schnullius, C. Predicting Forest Cover in Distinct Ecosystems: The Potential of Multi-Source Sentinel-1 and -2 Data Fusion. *Remote Sens.* **2020**, *12*, 302. [[CrossRef](#)]
66. Pascual, A.; Tupinambá-Simões, F.; Guerra-Hernández, J.; Bravo, F. High-Resolution Planet Satellite Imagery and Multi-Temporal Surveys to Predict Risk of Tree Mortality in Tropical Eucalypt Forestry. *J. Environ. Manag.* **2022**, *310*, 114804. [[CrossRef](#)]
67. Reiner, F.; Brandt, M.; Tong, X.; Skole, D.; Kariryaa, A.; Ciaï, P.; Davies, A.; Hiernaux, P.; Chave, J.; Mugabowindekwe, M.; et al. More than One Quarter of Africa’s Tree Cover Is Found Outside Areas Previously Classified as Forest. *Nat. Commun.* **2023**, *14*, 2258. [[CrossRef](#)]
68. Song, L.; Estes, A.B.; Estes, L.D. A Super-Ensemble Approach to Map Land Cover Types with High Resolution over Data-Sparse African Savanna Landscapes. *Int. J. Appl. Earth Obs. Geoinf.* **2023**, *116*, 103152. [[CrossRef](#)]
69. Kirillov, A.; Mintun, E.; Ravi, N.; Mao, H.; Rolland, C.; Gustafson, L.; Xiao, T.; Whitehead, S.; Berg, A.C.; Lo, W.-Y.; et al. Segment Anything 2023. *arXiv* **2023**, arXiv:2304.02643.
70. Osco, L.P.; Wu, Q.; de Lemos, E.L.; Gonçalves, W.N.; Ramos, A.P.M.; Li, J.; Junior, J.M. The Segment Anything Model (SAM) for Remote Sensing Applications: From Zero to One Shot 2023. *arXiv* **2023**, arXiv:2306.16623.
71. Quintero-Vallejo, E.; Benavides, A.M.; Moreno, N.; González-Caro, S. *Bosques Andinos, Estado Actual y Retos Para Su Conservación En Antioquia*, 1st ed.; Fundación Jardín Botánico de Medellín Joaquín Antonio Uribe—Programa Bosques Andinos (COSUDE): Medellín, Colombia, 2017; ISBN 978-958-59470-5-4.
72. Gómez-Ossa, L.; Botero-Fernández, V. Application of Artificial Neural Networks in Modeling Deforestation Associated with New Road Infrastructure Projects. *Dyna* **2017**, *84*, 68–73. [[CrossRef](#)]
73. Ibrahim, E.; Jiang, J.; Lema, L.; Barnabé, P.; Giuliani, G.; Lacroix, P.; Pirard, E. Cloud and Cloud-Shadow Detection for Applications in Mapping Small-Scale Mining in Colombia Using Sentinel-2 Imagery. *Remote Sens.* **2021**, *13*, 736. [[CrossRef](#)]
74. Brovelli, M.A.; Sun, Y.; Yordanov, V. Monitoring Forest Change in the Amazon Using Multi-Temporal Remote Sensing Data and Machine Learning Classification on Google Earth Engine. *ISPRS Int. J. Geo-Inf.* **2020**, *9*, 580. [[CrossRef](#)]
75. Norway’s International Climate and Forests Initiative (NICFI). *NICFI Satellite Data Program User Guide*; Norway’s International Climate and Forests Initiative (NICFI): Oslo, Norway, 2022.
76. Mohanty, S.P.; Czakon, J.; Kaczmarek, K.A.; Pyskir, A.; Tarasiewicz, P.; Kunwar, S.; Rohrbach, J.; Luo, D.; Prasad, M.; Fler, S.; et al. Deep Learning for Understanding Satellite Imagery: An Experimental Survey. *Front. Artif. Intell.* **2020**, *3*, 534696. [[CrossRef](#)]
77. Ren, H.; Liu, Y.; Chang, X.; Yang, J.; Xiao, X.; Huang, X. Mapping High-Resolution Global Impervious Surface Area: Status and Trends. *IEEE J. Sel. Top. Appl. Earth Obs. Remote Sens.* **2022**, *15*, 7288–7307. [[CrossRef](#)]
78. Karra, K.; Kontgis, C.; Statman-Weil, Z.; Mazzariello, J.; Mark, M.; Brumby, S. Impact Observatory, United States Global. Land Use/Land Cover with Sentinel-2 and Deep Learning. In Proceedings of the 2021 IEEE International Geoscience and Remote Sensing Symposium IGARSS, Brussels, Belgium, 11–16 July 2021.
79. Hansen, M.C.; Potapov, P.V.; Pickens, A.H.; Tyukavina, A.; Hernandez-Serna, A.; Zalles, V.; Turubanova, S.; Kommareddy, I.; Stehman, S.V.; Song, X.-P.; et al. Global Land Use Extent and Dispersion within Natural Land Cover Using Landsat Data. *Environ. Res. Lett.* **2022**, *17*, 034050. [[CrossRef](#)]
80. Martone, M.; Rizzoli, P.; Wecklich, C.; González, C.; Bueso-Bello, J.-L.; Valdo, P.; Schulze, D.; Zink, M.; Krieger, G.; Moreira, A. The Global Forest/Non-Forest Map from TanDEM-X Interferometric SAR Data. *Remote Sens. Environ.* **2018**, *205*, 352–373. [[CrossRef](#)]
81. Hansen, M.C.; Potapov, P.V.; Moore, R.; Hancher, M.; Turubanova, S.A.; Tyukavina, A.; Thau, D.; Stehman, S.V.; Goetz, S.J.; Loveland, T.R.; et al. High-Resolution Global Maps of 21st-Century Forest Cover Change. *Science* **2013**, *342*, 850–853. [[CrossRef](#)]
82. Shimada, M.; Itoh, T.; Motooka, T.; Watanabe, M.; Shiraiishi, T.; Thapa, R.; Lucas, R. New Global Forest/Non-Forest Maps from ALOS PALSAR Data (2007–2010). *Remote Sens. Environ.* **2014**, *155*, 13–31. [[CrossRef](#)]
83. Velasco, R.F.; Lippe, M.; Tamayo, F.; Mfuni, T.; Sales-Come, R.; Mangabat, C.; Schneider, T.; Günter, S. Towards Accurate Mapping of Forest in Tropical Landscapes: A Comparison of Datasets on How Forest Transition Matters. *Remote Sens. Environ.* **2022**, *274*, 112997. [[CrossRef](#)]
84. Diakogiannis, F.I.; Waldner, F.; Caccetta, P.; Wu, C. ResUNet-a: A Deep Learning Framework for Semantic Segmentation of Remotely Sensed Data. *ISPRS J. Photogramm. Remote Sens.* **2020**, *162*, 94–114. [[CrossRef](#)]

85. Murphy, K.P. *Machine Learning a Probabilistic Perspective*; MIT Press: Cambridge, MA, USA, 2013; ISBN 978-0-262-01802-9.
86. Chollet, F. Keras—Deep Learning Library 2015. Available online: <https://keras.io/> (accessed on 24 June 2023).
87. Abadi, M.; Agarwal, A.; Barham, P.; Brevdo, E.; Chen, Z.; Citro, C.; Corrado, G.S.; Davis, A.; Dean, J.; Devin, M.; et al. TensorFlow: Large-Scale Machine Learning on Heterogeneous Systems 2015. *arXiv* **2016**, arXiv:1603.04467.
88. Singh, D.; Singh, B. Investigating the Impact of Data Normalization on Classification Performance. *Appl. Soft Comput.* **2020**, *97*, 105524. [[CrossRef](#)]
89. IDEAM Leyenda Nacional de Coberturas de La Tierra. *Metodología CORINE Land Cover Adaptada Para Colombia Escala 1:100.000*; Instituto de Hidrología, Meteorología y Estudios Ambientales: Bogotá, Colombia, 2010.
90. Whitley, R.; Beringer, J.; Hutley, L.B.; Abramowitz, G.; De Kauwe, M.G.; Evans, B.; Haverd, V.; Li, L.; Moore, C.; Ryu, Y.; et al. Challenges and Opportunities in Land Surface Modelling of Savanna Ecosystems. *Biogeosciences* **2017**, *14*, 4711–4732. [[CrossRef](#)]
91. Srivastava, N.; Hinton, G.; Krizhevsky, A.; Sutskever, I.; Salakhutdinov, R. Dropout: A Simple Way to Prevent Neural Networks from Overfitting. *J. Mach. Learn. Res.* **2014**, *15*, 1929–1958.
92. Li, Y.; Zhang, H.; Xue, X.; Jiang, Y.; Shen, Q. Deep Learning for Remote Sensing Image Classification: A Survey. *WIREs Data Min. Knowl. Discov.* **2018**, *8*, e1264. [[CrossRef](#)]

**Disclaimer/Publisher’s Note:** The statements, opinions and data contained in all publications are solely those of the individual author(s) and contributor(s) and not of MDPI and/or the editor(s). MDPI and/or the editor(s) disclaim responsibility for any injury to people or property resulting from any ideas, methods, instructions or products referred to in the content.